Crystal and Electron Properties of Carbamazepine–Aspirin Co-crystal

Béatrice Nicolaï, Bertrand Fournier, Slimane Dahaoui, Jean-Michel Gillet, Nour-Eddine Eddine Ghermani

Article

Crystal and Electron Properties of Carbamazepine-Aspirin Co-crystal

Beatrice Nicolai, Bertrand Fournier, Slimane Dahaoui, Jean-Michel Gillet, and Nour-Eddine Ghermani

Cryst. Growth Des., **Just Accepted Manuscript** • DOI: 10.1021/acs.cgd.8b01698 • Publication Date (Web): 19 Dec 2018

Crystal and Electron Properties of Carbamazepine-Aspirin Co-crystal

Béatrice Nicolaï,[#,†] Bertrand Fournier,[⊥,†] Slimane Dahaoui[♣], Jean-Michel Gillet[†] and

Nour-Eddine Ghermani[*,⊥,†]

[#] Faculté de Pharmacie, Université Paris Descartes, 4 avenue de l'Observatoire, 75006 Paris, France

[⊥] Institut Galien Paris Sud, UMR CNRS 8612, Université Paris Sud, Université Paris Saclay Faculté de Pharmacie, 5, rue Jean-Baptiste Clément, 92296 Châtenay-Malabry, France.

†Laboratoire Structures, Propriétés et Modélisation des Solides (SPMS) UMR CNRS 8580, CentraleSupélec, Université Paris Saclay, 3 Rue Joliot Curie, 91190 Gif-sur-Yvette, France.

[♣]CRM^2, UMR CNRS 7036, Université de Lorraine, Faculté des Sciences et Techniques, BP 70239, Boulevard des Aiguillettes, 54506 Vandoeuvre-lès-Nancy CEDEX (France)

AUTHOR INFORMATION

Corresponding Author
*E-mail: noureddine.ghermani@u-psud.fr.
ORCID
Nour-Eddine Ghermani: 0000-0001-7180-6624
Notes
The authors declare no competing financial interest.

In memory of our colleague and friend Slimane Dahaoui who passed away in 2018, April, 28th.

ABSTRACT: Carbamazepine (CBZ) and aspirin (ASP) drug molecules in their 1:1 co-crystal interact by relatively strong hydrogen bonds and aromatic-aromatic contacts. The crystal structure and the experimental electron density in the CBZ:ASP co-crystal were derived from a high resolution X-ray diffraction experiment at 100 K and the results are compared to those previously obtained for the CBZ form III. The isobaric thermal expansion tensor appears to be much more anisotropic for the co-crystal than for CBZ form III. The thermal expansion coefficients α_V are found equal to 1.3 for CBZ III and 1.5×10^{-4} K^{-1} for CBZ:ASP co-crystal. The interactions in the CBZ:ASP co-crystal have also been analyzed through the electrostatic properties derived from both experimental and theoretical electron densities: topological features, atomic charges and electrostatic potential. A very good agreement was found for the values of the electron density at the critical points $\rho(\mathbf{r}_{CP})$ obtained from both experiment and theory. This is not, however, true for the Laplacian values which are systematically weaker in the theoretical approach. In contrast, the integrated atomic charges have higher magnitudes for the theoretical density. Additionally, it is shown here that the total molecular energies can be obtained from the electrostatic potential at the nuclei (EPN) within the Thomas-Fermi approximation. The best agreement with the conventional quantum calculations (Restricted Hartree-Fock RHF or Density Functional Theory DFT) was surprisingly obtained for the promolecule (superposition of Independent Atomic Model, IAM) density and not from the multipole model which overestimates or underestimates the energies.

INTRODUCTION

The design of multi-component crystals or co-crystals is a powerful technique to modify physico-chemical properties of active pharmaceutical ingredients (API's) such as solubility, chemical and physical stability, dissolution rate or hygroscopicity.[1-5] Traditionally, the properties of an API are modified by forming a salt but there is a limited number of available counter-ions and molecules with no acid or base functions are also difficult to ionize. A pharmaceutical co-crystal contains a therapeutic molecule with at least one counter molecule (or coformer), bound together via non-covalent intermolecular interactions. US Food and Drug Administration (FDA) provides a list of substances that have precedence as food ingredient ("generally recognized as safe" substance or GRAS). Moreover, multidrug co-crystals have been the subject of growing interest in the pharmaceutical industry because they may offer a tandem therapeutic effect. Recently the FDA approved the first multidrug co-crystal for chronic heart failure: Entresto gathers Sacubitril and Valsartan in a single dose.[6]

The general aim of crystal engineering is the understanding of the intermolecular interactions in a crystal packing for an ulterior design of new crystalline compounds with the desired physicochemical properties. The packing is described in terms of supramolecular synthons giving rise to particular spatial arrangements. Then, the goal of crystal engineering is also to recognize and design synthons that are robust enough to be exchanged from one crystalline structure to another. In early studies, hydrogen bond synthons have been identified in molecular crystals.[7] For this purpose, Etter *et al* proposed the concept of graph set annotations based on the geometric motifs of the hydrogen bond networks in the crystal structure.[8,9] Several other types of synthons have been identified, but their real implications in a crystal structure still remain subjective.[10] For example the strength of sandwich herringbone or stacking of aromatic

molecules are known to be rather weak but they appear to play an important role to establish stable packing arrangement.[10] Moreover, the same intermolecular interaction may be a constituent of different supramolecular synthons.

The solid state of carbamazepine (5H-Dibenzo[b,f]azepine-5-carboxamide) (hereafter CBZ), an antiepileptic drug (Tegretol®), has been extensively studied. CBZ is known to exhibit polymorphism (forms I, III, IV and V).[11-14] It has been recently revealed that form II of CBZ is in fact a THF solvate.[15-16] A survey of the Cambridge Structural Database (CSD) indicates that CBZ crystallizes in numerous solvated and co-crystal forms.[17] The analysis of the published crystalline structures indicates that the primary supramolecular synthon in CBZ is the carboxamide moiety ($CONH_2$). This chemical group most commonly forms a cyclic homosynthon with another CBZ molecule or cyclic heterosynthons (amide···acid but also amide···acid···H_2O etc.) with a carboxylic group such as that of aspirin. Aspirin (acetylsalycilic acid, hereafter ASP) is the well-known API used to treat pain, fever and inflammation.[18] Aspirin presents two crystalline forms, form II being found during attempts to obtain the co-crystal CBZ:ASP.[19] Indeed, it has been demonstrated that the crystallization of aspirin form II can occur in the presence of certain amides, such as in CBZ, whereas a co-crystallization with CBZ can also occur.[19] In the co-crystals of CBZ involving molecules with carboxylic acids, there are generally extensive hydrogen bonding networks as O-H···O, N-H···O, C-H···O and C-H···π but also aromatic group stackings.[18] CBZ co-crystals exhibit polymorphism as for CBZ-nicotinamide and CBZ-saccharin compounds.[20, 21] In the two forms of CBZ-saccharin, the crystal packings display both homosynthon (double hydrogen bonds involving the carboxamide group of CBZ) and heterosynthon (hydrogen bonds between the respective N-H and C=O moieties of CBZ and saccharine molecules) arrangements.

Accurate crystal structures and electron densities of CBZ III have been recently studied by X-ray and neutron diffraction experiments at 100 K.[22, 23] ASP electron density features were also reported from accurate X-ray data and theoretical calculations.[24] In the present paper, we present an analysis of the electron density in the 1:1 co-crystal CBZ:ASP (triclinic, $P\bar{1}$). In the crystallogenesis attempts of the CBZ III and this co-crystal, two new solvates of CBZ were fortuitously obtained. The thermal expansion of the co-crystal was analyzed from 100 K to ambient temperature and compared to that of pure CBZ III in order to get more insight into the preferred intermolecular interactions. The electron density of CBZ:ASP was derived from a high resolution X-ray diffraction at 100 K and from periodic theoretical calculations. Topological analysis based on Bader's theory of *Atoms In Molecules* (AIM) was carried out to characterize the covalent and hydrogen bonds in the crystal lattice.[25] The obtained atomic charges are discussed as well as the total energy of molecule derived from the electrostatic potential at the nuclei (EPN).

EXPERIMENTAL AND METHODOLOGICAL SECTION

Crystallization. White powders of carbamazepine (CBZ) and aspirin (ASP) were purchased from Spectrum & Cooper laboratories. Powder diffraction analyses of the commercial samples reveal that they correspond to form III of CBZ and form I of ASP. Prismatic single co-crystal CBZ:ASP (1:1 stoechiometry) was obtained by a slow evaporation at ambient temperature of a solution of CBZ with an excess of ASP (stoechiometry 1:2 in the solution) in ethyl acetate (CarloErba reagents). Other initial stoechiometries did not lead to single crystals of CBZ:ASP with suitable size for high resolution X-ray diffraction or to CBZ form III. During our several attempts to obtain a co-crystal, we never obtained the form II of aspirin contrary to what

was observed in a recent study.[26] Several solvents were tested, and a prismatic single crystal of an ethanol solvate of CBZ was obtained from an ethanol solution (absolute VWR Chemical, 99.7%) at room temperature and a prismatic single crystal of a solvate methanol was obtained from a methanol solution (CarloErba for HPLC-Plus-gradient, 99.9%) of CBZ and PEG400. We have fully determined the crystal structure (see Supplementary Information) of these solvates by single crystal X-ray diffraction and they were found to be isostructural to the THF solvate (former form II of CBZ).[15-16] The presence of water in the ethanol or methanol solvent leads systematically to the CBZ dihydrate.

X-ray data Collection. Diffraction data of the CBZ-ASP were collected at 100.0(2) K on a Kappa CCD APEX II diffractometer using graphite monochromated MoKα X-radiation. 17015 unique reflections were collected up to a resolution of $\sin\theta_{max}/\lambda = H/2 = 1.00$ Å^{-1} ($\theta = 45.5°$), where H is the Bragg vector modulus. An empirical absorption correction was applied using SADABS[26] computer program. SORTAV[27] program was used for sorting and averaging data revealing the good quality of the measurements (internal $R_{int} = 0.0442$ for a high data redundancy around 17). The details of the X-ray diffraction experiment and the crystallographic data for the CBZ:ASP co-crystal are given in Table 1.

Thermal expansion. The anisotropy of the intermolecular interactions can be investigated using the isobaric thermal expansion tensor, which is a measure of the interaction changes with temperature.[28,29] The tensor is calculated from the temperature-dependent cell parameters with the PASCAL program.[30] Details of the calculation procedure can be found elsewhere.[31] The thermal expansion tensor is a symmetrical second-rank tensor with nonzero diagonal eigenvalues α_{11}, α_{22}, α_{33}. A small value of an eigenvalue is commonly referred to a ‘‘hard’’ direction corresponding to a small deformation; conversely, a large value is associated to a ‘‘soft’’

direction i.e. a large deformation. The eigenvectors can be expressed as a function of the cell parameters *a*, *b* and *c*. The anisotropy of the thermal expansion can be expressed as a single value by the aspherism coefficient *A*, related to the three eigenvalues of the thermal tensor[32]

$$A(T) = \frac{2}{3}\sqrt{1 - \frac{3(\alpha_{11}\alpha_{22} + \alpha_{11}\alpha_{33} + \alpha_{22}\alpha_{33})}{\alpha_v^2}} \qquad (1)$$

with $\alpha_V = \frac{1}{V}\left(\frac{\partial V}{\partial T}\right)$, the thermal expansion coefficient, and *V* the unit cell volume. When *A* = 0, the thermal expansion is totally isotropic. The graphical representations of the tensor at a given temperature are drawn using WinTensor program.[33]

Spherical and Electron Density Refinements. The crystal structure of the CBZ:ASP compound was solved using SIR94 program[34] and refined using SHELX97[35] implemented in WinGX[36] package. For the electron density refinements, the Hansen-Coppens model[37] was used. The frozen core and normalized valence spherical densities are obtained from the Hartree-Fock wave functions of the free atoms or ions.[38] The aspherical part of the pseudo-atom electron density is described by the real normalized harmonics $y_{lm\pm}$ basis set (*l* = 0 (monopole) to 4 (hexadecapole)) and modulated by a Slater-type radial function $R_{nl}(r) = Nr^{n_l}\exp(-\xi_l r)$, where *N* is a normalization factor. The exponents ξ_l (in bohr^{-1}) of the radial functions are chosen equal to 3.18, 4.47, 3.84 and n_l = 2, 2, 3 up to octupoles (*l* = 3) for C, O and N atoms, respectively; ξ_l = 2.00 bohr^{-1} and n_l = 1 (dipole level, *l* = 1) for the hydrogen atoms.[39] MOPRO program[40, 41] was used for the refinements of the electron density $\rho(\mathbf{r})$. At the end of the refinement cycles, SHADE3 software was used to empirically estimate the anisotropic thermal parameters of hydrogen atoms.[42] These parameters were kept fixed to refine the electron density of CBZ:ASP compound.

Topological Analysis of the Electron Density. The topological features of the electron density were analyzed following the Bader's *Atoms in Molecules* theory.[25] This analysis allows a quantitative description of the bonds and the electronic structure of atoms in molecules. The gradient of the electron density $\nabla\rho(\mathbf{r}_{CP})$ vanishes at the critical points (CP) corresponding to the extrema (maximum and minimum) and saddle points of $\rho(\mathbf{r})$. Each CP is therefore characterized by two numbers: the number of the eigenvalues (for non-degenerate cases) and the signature of the eigenvalues triplet (λ_1, λ_2, λ_3). The ellipticity defined as $\varepsilon = (\lambda_1-\lambda_2)/\lambda_2$ is a quantitative measurement of the anisotropy of the electron density at the CP and reveals the character of the chemical bonds (σ or π).

Experimental Electrostatic Potential and Electrostatic Potential at the Nuclei (EPN). The electrostatic potential is based on the Hansen-Coppens electron density model.[37, 40, 41] The maps or the 3D views of the electrostatic potential reveal the nucleophilic (negative potential) and electrophilic (positive potential) regions of a molecule in relation with its chemical reactivity. The electrostatic potential can also be calculated at the nuclei positions. The expression of the electrostatic potential at the nucleus (EPN) have been extensively described by Coppens *et al.*[43] From the Hansen-Coppens model, only the monopole population (P_{val}) and its κ parameter contribute to the EPN since all higher multipoles of a given atom create a zero potential at its nucleus. Several molecular properties such as correlation energies in relation with the values of EPN have been described by Politzer *et al.*[44-45] Furthermore, the correlation between the EPN and the atomic or molecular energy was evaluated within the statistical approximation of Thomas-Fermi.[46-47] The proposed energy relation for the total energy of a system $E^{tot} = T + V$ (kinetic and potential energies) is

$$E^{tot} = \sum_A k_A Z_A V_{0,A} \qquad (2)$$

Z_A and $V_{0,A}$ are the nuclear charge and the potential at the nucleus of atom A, respectively; k_A is a proportional and adjustable factor for each atom A close to the value 3/7 suggested by the theory of Thomas-Fermi except for H atom (k_A = 0.531278).[46-47] The values obtained from the empirical equation (2) given above for the molecular energy of a set of several small organic molecules are in excellent agreement with those obtained by direct DFT calculations.[45-46] This theory was also recently reported in an excellent book.[48] In this work, our program POTNUC[49] was used to compute the electrostatic potential (EPN) $V_{0,A}$ at each nucleus A. From the values of EPN, the previous equation was used to estimate E^{tot} energy. Politzer has also proposed the decomposition of E^{tot} as

$$E^{tot} = \frac{3}{7}(E_{ne} + 2E_{nn}) \qquad (3)$$

where E_{ne} and E_{nn} are the total nuclear-electronic attraction and the total nuclear-nuclear repulsion energies, respectively.[46-47] E_{nn} is easy to calculate from the nuclear point charges, then an estimate of the total energy and that of nuclear-electronic interaction can be obtained from the equations (2) and (3). From the experimental electron density approach, a more detailed expression based on the multipole model was also given in the pioneering work of J. Bentley.[50]

Theoretical calculations. Periodic quantum-mechanical calculations using *CRYSTAL14* were performed using the DFT method with the B3LYP hybrid functional and two different basis sets: 6-31G(d,p) and cc-pvdz.[51-54] The crystal geometry from the refined charge density model has been used in these single-point calculations. The level of accuracy in evaluating the bi-electronic Coulomb and exchange series was controlled by five parameters for which the used values were chosen from 10^{-7} to 10^{-14}. The shrinking factor of the reciprocal space was set to 8,

corresponding to 260 k-points in the irreducible Brillouin zone. The convergence on total energy was managed with a threshold of 10^{-7}. The XFAC option was used to generate from the computed population matrix, the theoretical structure factors (hereafter *theoretical structure factors* TSF) on the set of the observed Miller indices (17015 data, see Table 1). Both basis sets yield the same results; hereafter we will only discuss those originating from the cc-pvdz one.

Non-periodic theoretical calculations were also performed using GAUSSIAN09.[55] The single-point calculations were managed on isolated molecules and on dimers considering the experimental molecular geometry. Different levels of theory have been considered: *(i)* restricted Hartree-Fock (RHF) with 6-31G basis set, *(ii)* density functional theory (DFT) method using the hybrid functional B3LYP with 6-31G(d,p) basis set and *(iii)* with cc-pvdz basis set. The total energies are given in *hartrees* (1 H = 1 atomic unit (a.u.) = 2625.5 kJ/mol). The experimental geometries were used as input.

RESULTS AND DISCUSSION

Crystal Structure. CBZ and ASP co-crystallize in the centrosymmetric P-1 space group, with one molecule of CBZ and one molecule of ASP in the asymmetric unit corresponding to a 1:1 stoechiometry in the solid state. The crystalline structure of this CBZ:ASP co-crystal has been solved in 2005 at room temperature and published together with the polymorph II of aspirin, but without a proper description of the crystalline structure.[19] The numbering schemes of the CBZ:ASP asymmetric unit are given Figure 1. Details on the crystallographic data and the refinements are listed in Table 1. Table 2 lists the main distances and angles obtained at the end of the multipole refinement of CBZ:ASP.

As in polymorphs I and IV of CBZ, there is a pyramidalization of the amide group NH_2 in the co-crystal: the N_1-C_{15}-N_2-H_{14} dihedral angle being -12.2(6)° which is lower than the one computed in the gas phase (-24.3°).[56] Previous periodic molecular modeling calculations also demonstrate that, in these carbamazepine polymorphs, the deformation of the amide geometry may occur in order to optimize hydrogen-bond interactions; and the neglect of the amide pyramidalization introduces significant errors in the crystal structure predictions for carbamazepine.[56]

In the co-crystal, both CBZ and ASP molecules act as a donor and an acceptor of hydrogen bond. The packing diagram shows an heterosynthon between the acid group COOH of aspirin and the carboxamide group ($CONH_2$) of CBZ and an additional heterosynthon between the acetyl group $COCH_3$ of aspirin and the NH_2 amine group of CBZ (see Figure 2). Consequently, two CBZ molecules and two ASP molecules form quadrimers with graph sets $D^1_1(2)$ for the two strong hydrogen bonds (O_2-$H_{25}\cdots O_1$, N_2-$H_{15}\cdots O_3$) and one weaker (N_2-$H_{14}\cdots O_5$, see Table 2 and Figure 2); each nitrogen atom is involved in a bifurcated H-bond with two different CBZ molecules. Besides these hydrogen bonds, weak CH···O (C_8-$H_8\cdots O_2$ and C_5-$H_5\cdots O_5$) interactions have also been found (Table 2). There are π–π interactions between the aromatic rings of the CBZ molecules forming the so-called sandwich herringbone (SH) stacking as found in CBZ III (Figure 2).[22] The ring centroid-centroid distances are found equal to 3.93 Å in CBZ:ASP and to 3.79 Å for CBZ III, respectively.

Thermal expansion of CBZ III and CBZ:ASP. The cell parameter values of the single crystals of CBZ form III and CBZ:ASP were determined from 100 K to ambient temperature with a step of 10 K. The variation of the cell parameters as a function of temperature for CBZ III

is in relatively good agreement with those previously published.[57] No phase transition was observed in both cases. The eigenvalues of the thermal expansion tensor have been compiled in Table 3 and the graphical representation of the tensor at ambient temperature is presented in Figure 2.[33] Since the cell parameters increase linearly with temperature, the isobaric thermal expansion tensor is constant with temperature.

All the unit cell parameters and volumes increase with temperature for CBZ III and CBZ:ASP co-crystal. Consequently, the thermal expansion is positive in all directions in both crystals (see Table 3 and Figure 2). The thermal expansion coefficients α_V are found equal to 1.3 and 1.5×10^{-4} K^{-1} for CBZ III and CBZ:ASP, respectively. These values are similar to that of L-ascorbic acid but smaller than the average value of 2.0×10^{-4} K^{-1} found for small organic molecules.[57, 58] The aspherism coefficient A, calculated according to equation 1, has a value of 0.49 for CBZ:ASP which is comparable to the one of tienoxolol and L-ascorbic acid.[58, 59] A small value of 0.28 was found for CBZ III indicating that the thermal expansion is more anisotropic in the co-crystal than in CBZ form III over the entire measured temperature range.

For the CBZ:ASP co-crystal, the main part of the expansion is along the eigenvector $\mathbf{e_3}$ (see Table 3, Figure 2). It is 4.5 to 25 times larger than the expansion along the two other axes. This high value emphasizes the "soft" direction in the crystal, along which the intermolecular interactions are the weakest; this $\mathbf{e_3}$ direction is more or less perpendicular to the infinite chains of quadrimers (see Figure 2).

In polymorph III of CBZ, each molecule of CBZ acts as donor and acceptor of hydrogen bonds: the molecules are involved in a dimeric homosynthon NH···O hydrogen bond (Figure 2). The two carboxamide groups of the CBZ molecules involved in a hydrogen bonded dimer are coplanar. There are SH (sandwich herringbone) aromatic interactions as shown in Figure 2 and

previously reported.[22] These aromatic group interactions between dimers of CBZ molecules also form infinite chains, however, unlike the co-crystal, these chains are along two different directions in approximately the ($\mathbf{e_1}$, $\mathbf{e_2}$) plane of tensor (see the dotted arrows in Figure 2). These chains are linked via weak CH···O hydrogen bonds and van der Waals interactions. The isobaric thermal expansion is almost isotropic in the ($\mathbf{e_2}$, $\mathbf{e_3}$) plane (see Figure 2 and Table 3) and is smaller along $\mathbf{e_1}$.

Electron Deformation Density Maps. Figure 3 depicts the experimental static electron deformation density maps obtained at the end of the multipole refinement. Different planes of CBZ and ASP molecules have been chosen (see Figure 1). The shared electrons in the single and double covalent bonds are clearly shown. On average, double bond in C=O or aromatic C=C bonds display a density peak value of 0.6 to 0.8 eÅ^{-3} whereas C-N and other C-C bonds have an average peak values ranging from 0.35 to 0.45 eÅ^{-3}. In the NH_2 group, the hydrogen atoms are characterized by higher dipoles (N_2-H_{14} and N_2-H_{15}) than those of the C-H groups in the aromatic rings. The oxygen lone pairs of O_1 and O_5 oxygen atoms are almost symmetrical in contrast to those of O_3 atom. This is clearly shown in the hydrogen bonds (N_2-H_{15}···O_3 and O_2-H_{25}···O_1, bottom of Figure 3). In the plane of this last map, O_3 display a higher lone pair directed toward the depletion of the electron density of atom C_{23} involved in the C_{23}=O_5 double bond.

In Figure 4, the electron deformation density obtained after the theoretical structure factors (TSF) refinement is depicted; Figures 3 and 4 display the same molecular parts for comparison. The peak bond accumulations are globally comparable for the covalent bonds. Discrepancies appear, however, for the oxygen lone pairs which are more populated and symmetrical in the theoretical maps, even for O_3 involved in strong hydrogen bonds (Bottom of

Figure 4). Moreover, the dipoles of H atoms are slightly less pronounced for the theoretical refinement especially for H_{14} and H_{15} atoms.

Topological Analysis of the Total Electron density. The total electron (core and valence) density has been characterized by its topological features reported in Table 4. The negativity of the Laplacian of the electron density in C-C, C=C, C=O, N-H, O-H and C-H bonds show the shared shell or covalent character. Conversely, in the hydrogen bonds and the $O_3\cdots O_4$ close contact (bottom of Table 4), the Laplacian is positive (close shell interaction) and low valued (from 0.7 to 4.2 e.Å^{-5}). For the peak height of the electron density at the bond critical points, the interacting chemical groups display the highest values: for CBZ molecule, C_{15}-O_1 (2.7 e.Å^{-3}) and C_{15}-N_1 and C_{15}-N_2 (2.2 e.Å^{-3}); for ASP molecule, C_{16}-O_3 (2.9 e.Å^{-3}), C_{16}-O_2 (2.3 e.Å^{-3}) compared to C_{23}-O_5 (2.9 e.Å^{-3}). As expected N-H and O-H groups exhibit higher values of $\rho(\mathbf{r}_{CP})$ (2.2 e.Å^{-3}for N_2-H_{14} and N_2-H_{15} bonds) compared to 2.1 e.Å^{-3} for O_2-H_{25} bond; on average 1.8 e. Å^{-3} was found for C-H bonds. All these values are in good agreement with those previously reported for CBZ III.[22] The values of $\rho(\mathbf{r}_{CP})$ at the bond critical points for hydrogen bonds and atomic close contact are obviously lower: 0.4 e.Å^{-3} for O_2-$H_{25}\cdots O_1$ and 0.1 e.Å^{-3}for N_2-$H_{15}\cdots O_3$ hydrogen bonds and for $O_3\cdots O_4$ contact (see Figure 1). These two last H-bonds display, however, different Laplacian values (2.4 *vs* 1.6 e.Å^{-5}). The oxygen atoms O_2 and O_5 are also involved in weaker C-H$\cdots$O intra-molecular hydrogen bonds: C_8-$H_8\cdots O_2$ ($\rho(\mathbf{r}_{CP})$ = 0.07 e.Å^{-3} and $\nabla^2\rho(\mathbf{r}_{CP})$ = 0.7 e.Å^{-5}) and C_5-$H_5\cdots O_5$ ($\rho(\mathbf{r}_{CP})$ = 0.05 e.Å^{-3} and $\nabla^2\rho(\mathbf{r}_{CP})$ = 0.8 e.Å^{-5}). In Table 4, the strength of the hydrogen bonds and atomic contacts was quantified by the interaction energies E_{NC} (for non-covalent (NC) interactions) which differentiate between O-H$\cdots$O (-81.9 kJ/mol), N-H$\cdots$O (-9.2 to -22.7 kJ/mol) and C-H$\cdots$O bonds (-6 kJ/mol on average).[60] In comparison, $O_3\cdots O_4$ intramolecular

contact interaction ($O_3 \cdots O_4$ = 2.74 Å < 2*$R_{van\ der\ Waals}$ = 2.80 Å) is characterized by E_{NC} = -14.4 kJ/mol). All these values are consistent with those reported for CBZ III.[22]

The topological analysis was also carried out from the theoretical structure factors (TSF) refinement density. The results are reported in Table 4 for comparison with the experimental features. There is a good agreement for the values of the electron density at the critical points $\rho(\mathbf{r}_{CP})$ obtained from the experiment and theory. However, differences between the two approaches appear in the absolute Laplacian values which are systematically weaker in the TSF refinement especially for C=O, O-H and N-H bonds: C16=O3 (-34.7 (exp) *vs* -26.2 (TSF) e.Å^{-5}), C23=O4 (-23.7 (exp) *vs* -17.7 (TSF) e.Å^{-5}), O2-H25 (-31.2 (exp) *vs* -26.8 (TSF) e.Å^{-5}), N2-H15 (-27.6 (exp) *vs* -22.0 (TSF) e.Å^{-5}). This remark holds true for the ellipticity ε values for the majority of the bonds. For the hydrogen bonds and intermolecular contacts, the Laplacian and non-covalent energy values obtained by both experiment and theory are in good agreement (bottom of Table 4).

Atomic Charges. The total electron density has been numerically integrated over the atomic basins for the two molecules in CBZ:ASP co-crystal.[25, 61,62] The values of the atomic charges are reported in Table 5. These charges were calculated for the CBZ$\cdots$ASP dimer (as in Figure 1). The charges of the most important atoms in the molecular interactions are highlighted in bold. The values obtained for CBZ molecule are globally in good agreement with those of CBZ III.[22] However, the absolute magnitudes of the atomic charges in CBZ III are higher than those for CBZ in the co-crystal: for example in CBZ III, 1.6, -0.9, -1.0 -0.9 e were obtained for atoms C_{15}, N_1, N_2, O_1, respectively.[22] H_{14} and H_{15} hydrogen atoms of the amine group of CBZ carry the same charges (0.4 to 0.5 e) in both crystalline structures. For the CBZ:ASP co-crystal,

the integrations of the atomic charges were also carried out for isolated molecules (Table 5). No significant differences of charges were found for the CBZ molecule in CBZ III and in the co-crystal. However, low values for isolated ASP molecule were observed for C_{23} (+1.0 *vs* +1.5 e), O_3 (-0.5 *vs* -0.8 e), O_4 (-0.6 *vs* -0.9 e), O5 (-0.7 *vs* -1.1 e) and H_{25} (+0.4 *vs* + 0.5 e) atoms. Looking at the sum of the atomic charges, no charge has been transferred between the two molecules in the co-crystal.

For comparison, the integrated charges obtained from Independent Atom Model (IAM) densities (promolecule) and from the theoretical structure factors (TSF) refinement are also reported in Table 5. As can be expected from a charge transfer consideration, the atomic charge absolute values from the promolecule are systematically weaker than those obtained from the experimental multipole refinement. Conversely, the atomic charges obtained from the theoretical approach are higher in their absolute values than those derived experimentally. This is particularly observed in CBZ molecule: C_{15} (1.62 e (TSF) *vs* 1.29 e (exp)), N_1 (-0.98 e (TSF) *vs* -0.70 e (exp)), N_2 (-1.17 e (TSF) *vs* -0.98 e (exp)), O_1 (-0.94 e (TSF) *vs* -0.71 e (exp)).

Electrostatic Potential. The electrostatic potential has been calculated around the isolated molecules and for the CBZ:ASP dimers in the co-crystal. Figure 5 illustrates the electrostatic potential using the iso-surface representation. For isolated CBZ (top of Figure 5), the negative region of electrostatic potential (nucleophilic part at -0.03 $eÅ^{-1}$ cut-off) is extended around the aromatic rings of the molecule showing the main contribution of the π-electrons. This also holds true for the ASP molecule; the proximity of the methyl group (positive contribution) to the carboxyl group counterbalances the negative contribution of the latter (at -0.03 $eÅ^{-1}$ cut-off). The electrostatic potential features of the CBZ:ASP dimers in the co-crystal are also displayed in

Figure 5. The aromatic-aromatic interaction between two CBZ molecules (sandwich herringbone (SH), also observed in the lattice of CBZ III[22]) is characterized by a large negative region of electrostatic potential surrounding the external part of the aromatic rings. For the CBZ···ASP dimer, at the chosen cut-off of -0.03 eÅ^{-1}, the negative potential still remains in the vicinity of the aromatic part of CBZ molecule. The right column of Figure 5 illustrates the electrostatic potential obtained from the theoretical structure factors refinement. For the same cut-offs, the negative theoretical electrostatic potential surfaces are more spatially extended for isolated molecules and for dimers.

Electrostatic Potential at the nuclei (EPN) and molecular total energies. Table 6 reports the values of the EPN obtained for each atom of the molecules in the CBZ:ASP co-crystal.[49] As mentioned before, only the parameters κ and P_{val} of the multipole model contribute to the EPN. For the sake of comparison, the values of EPN of the promolecules (sum of neutral atoms) and those obtained by the theoretical approach (TSF refinement) are also given. As for the atomic charges, the most important atoms in the molecular interactions are highlighted in bold in Table 6. It is worthy to note that the highest absolute EPN values are obtained from the theory for C, O, N elements and also H_{14}, H_{15} and H_{25} atoms (see Table 6), the remaining H atoms displaying close values between experiment and theory.

Equations (2) and (3) were used for estimating the total molecular energy E^{tot} (in *hartree*) from experimental and theoretical (TSF) approaches. The results are reported in Table 7 for isolated molecules and dimers and are compared to those obtained for CBZ III. The energy values of isolated or a group of molecules estimated with Gaussian software from RHF *6-31 G***, DFT B3LYP *6-31 G*** and DFT B3LYP *cc*-pvdz levels of theory are also given in Table 7.

These last two basis sets give very comparable values for the molecular energies. From the theoretical calculations, the interacting CBZ molecules in both CBZ III and CBZ:ASP co-crystal display the same average total energies: -1517.6 hartrees for RHF *6-31 G*** and -1526.3 hartrees for DFT B3LYP *6-31 G***. For comparison, the CBZ···ASP interaction is characterized by energy values of -1403.8 and -1411.5 hartrees for the two theoretical approaches. Table 7 also reports the energy estimates obtained after the experimental and TSF refinements. For both CBZ III and CBZ:ASP co-crystal, the multipole refinements over-estimate the total molecular energies. In CBZ:ASP co-crystal, we can notice that the TSF refinement leads systematically to the highest energies in absolute values. Surprisingly, the values derived from the "promolecule" density are those which are closest to the *ab initio* results especially those of DFT B3LYP (see Table 7).

CONCLUSIONS

The structure of the CBZ:ASP co-crystal was here described through the geometrical properties and also through the isobaric thermal expansion tensor. The comparison was made with the previous results of the CBZ form III crystal. Both crystal structures (CBZ and CBZ:ASP co-crystal) reveal strong hydrogen bonds and aromatic π-π interactions. CBZ III displays, however, a more isotropic thermal expansion tensor than that obtained for the CBZ:ASP co-crystal. This can be explained by several non-parallel molecular chains occurring in the former compound crystal lattice which both involve hydrogen bonding and π-π interactions. The electron densities were here derived from X-ray and theoretical structure factors based on the experimental geometry using the B3LYP/cc-pvdz quantum chemistry model. The deformation electron density maps obtained from these two approaches are very comparable for the covalent bonds except for

the oxygen lone pairs and for the polarization of aromatic H atoms. The topological features of the total electron density in the CBZ:ASP co-crystal were carefully analyzed. The values of the electron density at the bond critical points (BCP) obtained for the experiment and theory are similar. A disagreement on the Laplacian estimates at the BCP was observed; for all covalent bonds, the theoretical Laplacian values are systematically slightly lower than those derived from the experiment. For the hydrogen bonds and atomic contacts, however, all the topological features are comparable. The integrated atomic charges were here estimated from the total electron densities. The refinement against the TSF gives systematically higher magnitudes of the atomic charges than those derived from the experimental structure factors. The same trend was observed for the electrostatic potential derived from the TSF refinement which displays more extended negative potential regions around the isolated molecules and the dimers in the CBZ:ASP co-crystal. This feature also shows that the aromatic π-electron contribution is significantly enhanced in the TSF refinement. The electrostatic potential at the nuclei (EPN) was used here to estimate the total molecular energy following the Politzer *et al* approximation.[44-46] The best agreement to reproduce the quantum *ab initio* total energy was here obtained with the IAM electron density (promolecule) and not from the multipole refinements. Investigations to elucidate this issue are in progress.

ASSOCIATED CONTENT

Supporting Information

Residual density maps after the multipole refienement, crystal data and structures of ethanol and methanol solvates of carbamazepine are available free of charge via the internet at http://pubs.acs.org. CCDC 1877787 contains the supplementary crystallographic data for this paper. These data can be obtained free of charge from The Cambridge Crystallographic Data Centre via www.ccdc.cam.ac.uk/structures/.

ACKNOWLEDGMENT

The CNRS, Université Paris Saclay, Université Paris Sud, Université Paris Descartes, Université de Lorraine and Ecole CentraleSupélec are acknowledged.

REFERENCES

(1) Desiraju, G. R. Crystal and co-crystal. *Cryst. Eng. Comm.* **2003**, *5*, 466-467.

(2) Dunitz, J. D. Crystal and co-crystal: a second opinion. *Cryst. Eng. Comm.* **2003**, *5*, 506-506.

(3) Bond, A. D. What is a co-crystal? *Cryst. Eng. Comm.* **2007**, *9*, 833-834.

(4) Jones, W.; Motherwell, S.; Trask, A.V. Pharmaceutical cocrystals: an emerging approach to physical property enhancement. *Pharm. Mat. Sci.* **2006**, *31(11),* 875-879.

(5) Schultheiss, N.; Newman, A. Pharmaceutical cocrystals and their physicochemical properties. *Cryst. Growth Des.* **2009**, *9,* 2950-2967.

(6) Fala, L. Entresto (sacubitril/valsartan): frist-in-class angiotensin receptor neprilysin inhibitor FDA approved for patients with heart failure. *American Health and Drug Benefits* **2015**, *8*, 330-334.

(7) Etter, M. C. Hydrogen bonds as design elements in organic chemistry. *J. Phys. Chem.* **1991**, *95*, 4601-4610.

(8) Etter, M. C. Encoding and decoding hydrogen-bond patterns of organic compounds. *Acc. Chem. Res.* **1990**, *23,* 120-126.

(9) Etter, M. C.; Macdonald, J.C.; Bernstein, J. Graph-set analysis of hydrogen-bond patterns in organic crystals. *Acta Crystallogr.* **1990**, *B46*, 256-262.

(10) Desiraju, G. R. Supramolecula synthons in crystal engineering- a new organic synthesis. *Angew. Chem. Int. Ed.* **1995**, *34*, 2311-2327.

(11) Grzesiak, A. L.; Lang, M. D.; Kim, K.; Matzgeret, A.J. Comparison of the four anhydrous polymorphs of carbamazepine and the crystal structure of form I. *J. Pham. Sci.* **2003**, *92*, 2260-2271.

(12) Reboul, J. P.; Cristau, B.; Soyfer, J. C.; Astier, J. P. 5H-dibenz[b,f]azépinecarboxamide-5 (carbamazepine). *Acta Crystallogr.* **1981**, *B37*, 1844-1848.

(13) Lang, M.; Kampf, J. W.; Matzger, A. J. Form IV of carbamazepine. *J. Pham. Sci.* **2002**, *91*, 1187-1190.

(14) Arlin, J. B., Price, L. S.; Price, S. L.; Florence, A. J. A strategy for producing predicted polymorphs: catemeric carbamazepine form V. *Chem. Comm.* **2011**, *47*, 7074-7076.

(15) Lowes, M. M. J.; Cairo, M. R.; Lötter, A. P.; van der Watt, J.G. Physicochemical properties and x-ray structural studies of the trigonal polymorph of carbamazepine. *J. Pharm. Sci.* **1987**, *76*, 744-752.

(16) Fabbiani, F. P. A.; Byrne, L. T.; Mckinnon, J. J.; Spackman, M. A. Solvent inclusion in the structural voids of form II carbamazepine: single-crystal X-ray diffraction, NMR spectroscopy and Hirshfeld surface analysis. *Cryst. Eng. Comm.* **2007**, *9*, 728-731.

(17) Groom, C. R.; Bruno, I. J.; Lightfoot, M. P.; Ward S. C. The Cambridge Structural Database. *Acta Crystallogr.* **2016**, *B72*, 171-179.

(18) Fu, Q.; Han, Y.; Xie, Y.-f.; Gong, N.-b.; Guo, F. Carbamazepine cocrystals with several aromatic carboxylic acids in different stoechiometries: structures and solid state characterization. *J. Mol. Struct.* **2018**, *1168*, 145-152.

(19) Vishweshwar, P.; McMahon, J. A.; Oliveira, M.; Peterson, M. L.; Zaworotko, M. J. The predictably elusive form II of aspirin. *J. Am. Chem. Soc.* **2005**, *127*, 16802-16803.

(20) Porter III, W. W.; Elie, S. C.; Matzger, A. J. Polymorphism in carbamazepine cocrystals. *Cryst. Growth Des.* **2008**, *8*, 14-16.

(21) Jayasankar, A.; Somwangthanaroj, A.; Shao, Z. J.; Rodrıguez-Hornedo N. Cocrystal formation during cogrinding and storage is mediated by amorphous phase. *Pharm. Res*. **2006**, *23*, 2381-2392.

(22) El Hassan, N.; Ikni, A.; Gillet, J.-M.; Spasojevic-de Biré, A.; Ghermani., N. E. Electron properties of carbamazepine drug in form III. *Cryst. Growth Des.* **2013**, *13*, 2887-2896.

(23) Sovago, I.; Gutmann, M. J.; Senn, H. M.; Thomas, L. H.; Wilson, C. C.; Farrugia, L. J. Electron density, disorder and polymorphism: high-resolution diffraction studies

of the highly polymorphic neuralgic drug carbamazepine. *Acta Crystallogr.* **2016**, *B72*, 39-50.

(24) Arputharaj, D. S.; Hathwar, V. R.; Row, T. N. G.; Kumaradhas, P. Topological electron density analysis and electrostatic properties of aspirin: experimental and theoretical study. *Cryst. Growth Des.* **2012**, *12*, 4357-4366.

(25) Bader, R. F. W. *Atoms in Molecules – A Quantum Theory*; Clarendon Press: Oxford, **1990**.

(26) *SADABS* (Version 2.10). George Sheldrick, University of Göttingen, **2003**.

(27) Blessing, R. H. Outlier treatment in data merging. *J. Appl. Crystallogr.* **1997**, *30*, 421-426.

(28) Salud, J.; Barrio, M.; Lopez, D. O.; Tamarit, J. L.; Alcobe, X. Anisotropy of intermolecular interactions form the study of the thermal-expansion tensor. *J. Appl. Crystallogr.* **1998,** *31*, 748-757.

(29) Weigel, D.; Beguemsi, T.; Garnier, P.; Berar, J. F Evolution des tenseurs de dilatation thermique en fonction de la température.I. Loi générale d'évolution de la symétrie du tenseur. *J. Sol. Stat. Chem.* **1978,** *23*, 241-251.

(30) Cliffe, M. J.; Goodwin, A. L. Pascal : a principal axis strain calculator for thermal expansion and compressibility determination. *J. Appl. Crystallogr.* **2012,** *45*, 1321-1329.

(31) Physical properties of crystals. In International tables for crystallography D:, Authier, A., Ed. Kluwer, Dordrecht, **2006**; Vol. 1.4.

(32) Parat, B.; Pardo, L. C.; Barrio, M.; Tamarit, J. L.; Negrier, P.; Salud, J.; Lopez, D. O.; Mondieig, D. Polymorphism of $CBrCl_3$. *Chem. Mat.* **2005**, *17*, 3359-3365.

(33) Kaminski, W. WinTensor (http://cad4.cpac.washington.edu/wintensorhome/wintensor.htm), 1.1; 2004.

(34) Altomare, A.; Cascarano, G.; Giacovazzo, C.; Guagliardi, A. Completion and refinement of crystal structures with SIR92. *J. Appl. Crystallogr.* **1993**, *26*, 343-350.

(35) Sheldrick, G. M. A Short History of SHELX. *Acta Crystallogr.* **2008**, *A64*, 112-122.

(36) Farrugia, L. J. *WinGX* suite for small-molecule single-crystal crystallography. *J. Appl. Crystallogr.* **1999**, *32*, 837-838.

(37) Hansen, N. K.; Coppens, P. Testing aspherical atom refinements on small-molecule data sets. *Acta Crystallogr.* **1978**, *A34*, 909-921.

(38) Clementi, E.; Roetti, C. Atomic data and Nuclear data tables. Academic press, New York, USA, **1974**, *14*, 177.

(39) Clementi, E.; Raimondi, D.L. Atomic screening constants from SCF functions. *J. Chem. Phys.* **1963**, *41*, 2686.

(40) Guillot, B.; Viry, L.; Guillot, R.; Lecomte, C.; Jelsch, C. Refinement of proteins at subatomic resolution with MOPRO. *J. Appl. Crystallogr.* **2001**, *34*, 214-223.

(41) Jelsch, C.; Guillot, B.; Lagoutte, A.; Lecomte, C. *J.* Advances in Proteins and Small Molecules. Charge Density Refinement Methods using software MoPro. *Appl. Crystallogr.* **2005**, *38*, 38-54.

(42) Madsen, A. O. *J.* SHADE web server for estimation of hydrogen anisotropic displacement parameters. *Appl. Crystallogr.* **2006**, *39*, 757-758.

(43) Volkov, A.H.; King, F.; Coppens, P.; Farrugia, L. J. On the calculation of the electrostatic potential, electric field and electric field gradient from the aspherical pseudoatom model. *Acta Crystallogr.* **2006**, *A62*, 400-408.

(44) Politzer, P. Observations on the significance of the electrostatic potentials at the nuclei of atoms and molecules. *Israel J. Chem.* **1980**, *19*, 224-232.

(45) Politzer P.; Levy, M. Energy differences from electrostatic potentials at nuclei. *J. Chem. Phys.* **1987**, *87*, 5044-5046.

(46) Politzer, P.; Lane, P.; M. C. Concha, M. C. Atomic and molecular energies in terms of electrostatic potentials at nuclei. *Int. J. Quant. Chem.* **2002**, *90*, 459-463.

(47) Chai, J.-D.; Head-Gordon, M. Long-range corrected hybrid density functionals with damped atom–atom dispersion corrections. *Phys. Chem. Chem. Phys.* **2008**, *10*, 6615-6620.

(48) Brändas, E. J.; Kryachko, E. S. *Quantum Chemistry: A tribute to the memory of Per-Olov Löwdin*. KLUWER ACADEMIC PUBLISHERS. The Netherlands. 2003.

(49) ELECTROS, STATDENS, FIELD, POTNUC: Computer programs to calculate electrostatic properties from high resolution X-ray diffraction. Internal report UMR CNRS 7036, Université Henri Poincaré, Nancy 1, France and Institut Galien Paris Sud, UMR CNRS 8612, Université Paris-Sud, France and Université Cadi Ayyad, Morocco (1992-2018). N. E. Ghermani, N. Bouhmaida and C. Lecomte.

(50) Bentley, J. Determination of electronic energies from experimental electron densities. *J. Chem. Phys.* **1979**, *70*, 159-164.

(51) Dovesi, R.; Orlando, R.; Erba, A.; Zicovich-Wilson, C. M. ; Civalleri, B. ; Casassa, S.; Maschio, L.; Ferrabone, M.; De La Pierre, M.; D'Arco, P.; Noël, Y.; Causà, M.; Rérat, M.; Kirtman, B. CRYSTAL14: A program for the ab initio investigation of crystalline solids. *Int. J. Quant. Chem.* **2014**, *114*, 1287–1317.

(52) Hohenberg, P.; Kohn, W. Inhomogeneous electron gas. *Phys. Rev.* **1964**, *B136*, 864-871.

(53) Lee, C.; Yang, W.; Parr, R.G. Development of the Colle-Salvetti correlation-energy formula into a functional of the electron density. *Phys. Rev. B* **1988**, *37*, 785-789.

(54) Hariharan, P.C.; Pople, J.A. The influence of polarization functions on molecular orbital hydrogenation energies. *Th. Chim. Acta* **1973**, *28*, 213-222.

(55) Gaussian 09, Revision A.1, Frisch, M. J.; Trucks, G. W.; Schlegel, H. B.; Scuseria, G. E.; Robb, M. A.; Cheeseman, J. R.; Scalmani, G.; Barone, V.; Mennucci, B.; Petersson, G. A.; Nakatsuji, H.; Caricato, M.; Li, X.; Hratchian, H. P.; Izmaylov, A. F.; Bloino, J.; Zheng, G.; Sonnenberg, J. L.; Hada, M.; Ehara, M.; Toyota, K.; Fukuda, R.; Hasegawa, J.; Ishida, M.; Nakajima, T.; Honda, Y.; Kitao, O.; Nakai, H.; Vreven, T.; Montgomery, Jr., J. A.; Peralta, J. E.; Ogliaro, F.; Bearpark, M.; Heyd, J. J.; Brothers, E.; Kudin, K. N.; Staroverov, V. N.; Kobayashi, R.; Normand, J.; Raghavachari, K.; Rendell, A.; Burant, J. C.; Iyengar, S. S.; Tomasi, J.; Cossi, M.; Rega, N.; Millam, J. M.; Klene, M.; Knox, J. E.; Cross, J. B.; Bakken, V.; Adamo, C.; Jaramillo, J.; Gomperts, R.; Stratmann, R. E.; Yazyev, O.; Austin, A. J.; Cammi, R.; Pomelli, C.; Ochterski, J. W.; Martin, R. L.; Morokuma, K.; Zakrzewski, V. G.; Voth, G. A.; Salvador, P.; Dannenberg, J. J.; Dapprich, S.;

Daniels, A. D.; Farkas, Ö.; Foresman, J. B.; Ortiz, J. V.; Cioslowski, J.; Fox, D. J. Gaussian, Inc., Wallingford CT, 2009.

(56) Cruz Cabeza, A. J.; Day, G. M.; Motherwell, S.; Jones, W. Amide pyramidalization in carbamazepine: a flexibility problem in crystal structure prediction? *Cryst. Growth Des.* **2006**, *6*, 1858-1866.

(57) Brandenburg, J. G.; Potticary, J.; Sparkes, H. A.; Price, S. L.; Hall, S. R. Thermal expansion of carbamazepine: Systematic crystallographic measurements challenge quantum chemical calculations. *Phys. Chem. Lett.* **2017**, *8*, 4319-4324.

(58) Nicolai, B.; Barrio, M.; Tamarit, J.-L.; Céolin, R.; Rietveld, I. B. Thermal expansion of L-ascorbic acid. *Eur. Phys. J.* **2017**, *226*, 905-912.

(59) Nicolaï, B.; Rietveld, I. B.; Barrio, M.; Mahé, N.; Tamarit, J.-L.; Céolin, R.; Guéchot, C.; Teulon, J.-M. Uniaxial negative thermal expansion in crystals of tienoxolol. *Struct. Chem.* **2013**, *24*, 279-283.

(60) Espinosa, E.; Molins, E.; Lecomte C. Hydrogen bond strengths revealed by topological analyses of experimentally observed electron densities. *Chem. Phys. Lett.* **1998**, *285*, 170-173.

(61) Henkelman, G.; Arnaldsson, A.; Jonsson, H. A fast and robust algorithm for Bader decomposition of charge density. *Comput. Mater. Sci.* **2006**, *36*, 354-360.

(62) Tang, W.; Sanville, E.; Henkelman, G. A grid-based Bader analysis algorithm without lattice bias. *J. Phys.: Condens. Matter,* **2009***, 21*, 084204.

Table 1. Data Collection and Refinement Details of CBZ:ASP Co-crystal.

Empirical formula	$C_{24}H_{20}N_2O_5$
Formula weight	1960.87
Temperature (K)	100.0(2)
Crystal system	Triclinic
Space group	P-1

Unit cell dimensions	a = 9.0161(1) Å b = 11.3400(2) Å c = 11.4142(2) Å α = 60.340(2)° β = 85.622(2)° γ = 84.722(2)°
Volume	1009.17(3) Å^3
Z	2
Density (calculated) (Mg/m^3)	1.370
Absorption coefficient (mm^{-1})	0.097
F(000)	436
Reflections collected	292549
Independent reflections	17015 [R_{int} = 0.0442]
Completeness to θ = 45.51°	92.8%
Spherical Refinement	
R_1, wR_2, gof [I>2sigma(I)]	3.39 %, 7.35 %, 0.81
Multipole Refinement	
R_1(F), wR_2(F), gof [I>2sigma(I)]	2.69 %, 3.00 %, 1.53 1.00 %, 0.36 %, 3.26*

**refinement against 17015 theoretical structure factors (TSF) from cc-*pvdz *basis set.*

Table 2. Selected Bond Lengths (Å), Angles and Torsion Angles (deg) in CBZ:ASP Co-crystal.

CBZ			
C15-O1	1.2490(6)	O1-C15-N2	122.26(4)
C15-N2	1.3471(9)	C1-N1-C14	116.94(3)
C15-N1	1.3657(6)	C6-C7-C8	126.73(5)
C1-N1	1.4264(9)	C7-C8-C9	127.45(4)
C14-N1	1.4287(7)	C1-C6-C7	123.40(5)
		C8-C9-C14	119.17(3)
C1-C2	1.3921(12)	C1-N1-C15-O1	-8.92(3)
C1-C6	1.4002(10)	C1-N1-C15-N2	172.85(4)
C2-C3	1.3911(9)	C1-N1-C14-C13	113.75(5)
C3-C4	1.3972(11)	C1-N1-C14- C9	-67.40(4)
C4-C5	1.3875(12)	N1-C15-N2-H14	-12.2(6)
C5-C6	1.4033(9)	N1-C15-N2-H15	-175.0(2)
C6-C7	1.4581(13)		
C7-C8	1.3513(8)		
C8-C9	1.4578(10)		
C9-C10	1.4035(7)		
C9-C14	1.4017(11)		
C10-C11	1.3853(10)		
C11-C12	1.3938(11)		
C12-C13	1.3903(7)		
C13-C14	1.3923(9)		
ASP			
C23-O5	1.2047(10)	O2-C16-O3	123.04(5)
C16-O3	1.2197(6)	C22-C17-C18	118.07(5)
C16-O2	1.3197(9)	O4-C22-C17	121.36(5)
C23-O4	1.3562(9)	C23-O4-C22	120.63(3)
C22-O4	1.3850(8)		
C16-C17	1.4875(6)	C18-C17-C16-O2	-11.87(4)
C17-C18	1.4017(8)	C18-C17-C16-O3	167.91(4)
C17-C22	1.4014(8)	C17-C22-O4-C23	80.40(4)
C18-C19	1.3887(6)	C22-O4-C23-C24	-168.60(4)
C19-C20	1.3943(9)		
C20-C21	1.3904(8)		
C21-C22	1.3883(6)		
C23-C24	1.4929(9)		
Hydrogen bonds			
H25…O1[1]	1.601(7)	O2-H25…O1	168.18(19)
H15…O3[1]	1.913(6)	N2-H15…O3	167.65(14)
H14…O5[2]	2.243(6)	N2-H14…O5	152.45(14)
H8…O2[3]	2.568(6)	C8-H8…O2	157.57(19)
H5…O5[3]	2.510(6)	C5-H5…O5	144.9(4)

symmetry operations : [1]-x,-y, 2-z ; [2]1+x, y, z ; [3] x, y, z

Table 3. Eigenvalues (α_{ii}), Eigenvectors (e_i with respect to the Cell Vectors a, b, c) and Aspherism Coefficient A of the Isobaric Thermal Expansion Tensors of CBZ III and CBZ:ASP Co-crystal.

	CBZ III	*CBZ:ASP*
α_{11} (MK^{-1})	27.1(31)	4.3(21)
α_{22} (MK^{-1})	46.3(29)	24.3(36)
α_{33} (MK^{-1})	47.5(26)	111.1(35)
$\mathbf{e_1}$	-0.994**a** + 0.110**c**	0.370**a** + 0.901**b** + 0.227**c**
$\mathbf{e_2}$	1.0**b**	0.906**a** - 0.388**b** + 0.171**c**
$\mathbf{e_3}$	0.418**a** + 0.908**c**	-0.261**a** - 0.484**b** + 0.835**c**
α_V (MK^{-1})	131.6(8)	147.8(8)
A	0.28	0.49

Table 4. Topological Properties of the Electron Density of CBZ:ASP Cocrystal.[a] The first and second Lines correspond to the values obtained from the experimental Electron Density and from the Theoretical Structure Factors (TSF) refinement, respectively.

bond A-B	*d*(CP-A) (Å)	*d*(CP-b) (Å)	$\rho(\underline{r}_{CP})$ (e.Å^{-3})	$\nabla^2\rho(\underline{r}_{CP})$ (e.Å^{-5})	ε
CBZ					
C15-O1	0.458	0.791	2.69	-34.0	0.120
	0.460	0.790	2.63	-27.7	0.131
C15-N2	0.533	0.814	2.25	-26.9	0.171
	0.554	0.794	2.29	-23.7	0.190
C15-N1	0.558	0.808	2.21	-24.2	0.212
	0.570	0.795	2.20	-20.6	0.216
C1-N1	0.599	0.827	1.87	-15.2	0.051
	0.599	0.827	1.86	-13.1	0.050
C14-N1	0.606	0.823	1.84	-13.7	0.055
	0.608	0.821	1.87	-12.7	0.034
C1-C2	0.678	0.715	2.16	-20.7	0.290
	0.724	0.668	2.08	-17.8	0.262
C1-C6	0.702	0.699	2.11	-19.9	0.266
	0.718	0.682	2.07	-17.6	0.203
C2-C3	0.712	0.680	2.12	-19.9	0.241
	0.669	0.722	2.10	-18.2	0.193
C3-C4	0.689	0.708	2.11	-19.4	0.221
	0.710	0.687	2.06	-17. 5	0.217
C4-C5	0.707	0.680	2.16	-21.1	0.198
	0.681	0.707	2.09	-18.1	0.189
C5-C6	0.701	0.703	2.09	-19.6	0.192
	0.709	0.695	2.03	-16.3	0.179
C6-C7	0.732	0.726	1.84	-14.3	0.147
	0.731	0.727	1.85	-13.3	0.114
C7-C8	0.668	0.684	2.34	-23.0	0.293
	0.679	0.673	2.26	-21.6	0.309
C8-C9	0.750	0.708	1.84	-14.6	0.127
	0.738	0.720	1.84	-13.4	0.142
C9-C10	0.695	0.709	2.07	-18.4	0.161
	0.714	0.689	2.04	-16.8	0.180
C9-C14	0.676	0.726	2.04	-18.0	0.259
	0.701	0.701	2.07	-17.5	0.233
C10-C11	0.683	0.703	2.14	-20.3	0.191
	0.692	0.693	2.13	-17.8	0.228
C11-C12	0.718	0.676	2.13	-20.4	0.195
	0.673	0.721	2.09	-17.7	0.197
C12-C13	0.681	0.709	2.11	-20.2	0.178
	0.695	0.696	2.09	-17.9	0.228
C13-C14	0.692	0.700	2.11	-19.9	0.234
	0.674	0.719	2.12	-18.6	0.238
N2-H14	0.733	0.275	2.22	-28.9	0.067
	0.758	0.250	2.10	-25.2	0.075
N2-H15	0.725	0.290	2.24	-27.6	0.076
	0.757	0.258	2.04	-22.0	0.079
C2-H2	0.702	0.380	1.83	-18.4	0.086
	0.716	0.366	1.83	-16.3	0.006
C3-H3	0.717	0.360	1.79	-17.6	0.055
	0.715	0.362	1.85	-17.7	0.058
C4-H4	0.703	0.376	1.82	-18.7	0.003
	0.704	0.375	1.79	-15.7	0.000
C5-H5	0.718	0.356	1.80	-17.9	0.077
	0.713	0.362	1.84	-17.4	0.053
C7-H7	0.694	0.384	1.80	-17.9	0.040
	0.719	0.359	1.82	-16.3	0.032

C8-H8	0.673	0.413	1.78	-16.9	0.025
	0.720	0.366	1.81	-15.8	0.033
C10-H10	0.674	0.401	1.78	-17.2	0.070
	0.700	0.375	1.85	-16.8	0.046
C11-H11	0.716	0.364	1.84	-19.2	0.043
	0.709	0.371	1.83	-17.2	0.016
C12-H12	0.703	0.376	1.84	-19.0	0.033
	0.707	0.372	1.86	-17.9	0.039
C13-H13	0.709	0.369	1.84	-19.0	0.071
	0.714	0.364	1.81	-16.7	0.038
ASP					
C23-O5	0.416	0.789	2.93	-26.2	0.134
	0.425	0.780	2.93	-27.2	0.139
C16-O3	0.437	0.783	2.90	-34.7	0.131
	0.434	0.786	2.80	-26.2	0.108
C16-O2	0.497	0.822	2.27	-26.8	0.102
	0.508	0.813	2.23	-22.2	0.096
C23-O4	0.507	0.850	2.06	-23.7	0.050
	0.535	0.822	2.03	-17.7	0.093
C22-O4	0.550	0.837	1.90	-15.7	0.008
	0.557	0.828	1.84	-11.2	0.023
O2-H25	0.753	0.217	2.13	-31.2	0.031
	0.761	0.210	2.12	-26.8	0.009
C16-C17	0.772	0.715	1.81	-14.1	0.158
	0.780	0.708	1.79	-13.0	0.157
C17-C18	0.704	0.698	2.07	-18.4	0.220
	0.694	0.708	2.03	-16.2	0.198
C17-C22	0.685	0.716	2.13	-19.3	0.232
	0.684	0.718	2.06	-17.1	0.241
C18-C19	0.688	0.701	2.15	-20.0	0.205
	0.712	0.677	2.09	-17.8	0.208
C19-C20	0.680	0.715	2.14	-19.4	0.211
	0.682	0.713	2.10	-18.1	0.149
C20-C21	0.714	0.676	2.12	-19.5	0.218
	0.691	0.700	2.09	-17.5	0.182
C21-C22	0.679	0.710	2.17	-20.6	0.245
	0.667	0.721	2.13	-18.5	0.224
C23-C24	0.795	0.698	1.75	-13.8	0.113
	0.803	0.690	1.76	-12.2	0.095
C18-H18	0.712	0.369	1.80	-18.4	0.067
	0.710	0.370	1.81	-16.6	0.047
C19-H19	0.698	0.379	1.83	-19.0	0.033
	0.710	0.368	1.80	-15.5	0.054
C20-H20	0.730	0.348	1.79	-18.7	0.065
	0.711	0.366	1.81	-16.2	0.034
C21-H21	0.711	0.373	1.86	-18.8	0.051
	0.706	0.377	1.78	-15.3	0.037
C24-H22	0.716	0.360	1.67	-14.2	0.074
	0.699	0.377	1.80	-15.7	0.010
C24-H23	0.703	0.375	1.75	-16.8	0.076
	0.689	0.389	1.83	-16.6	0.005
C24-H24	0.707	0.365	1.75	-17.4	0.028
	0.700	0.371	1.76	-15.3	0.023

Hydrogen bonds and intermolecular contacts						E_{NC}
O2-H25…O1[1]	0.523	1.078	0.38	4.2	0.006	-81.9
	0.519	1.083	0.34	5.6	0.010	-77.2
N2-H15…O3[1]	0.666	1.261	0.14	2.4	0.197	-22.7
	0.685	1.230	0.16	3.0	0.023	-27.8
N2-H14…O5[2]	0.865	1.401	0.07	1.2	0.295	-9.2
	0.868	1.392	0.07	1.4	0.141	-9.6
C8-H8…O2[3]	1.082	1.517	0.07	0.7	0.495	-6.3
	1.059	1.595	0.04	0.8	0.824	-4.8
C5-H5…O5[3]	1.064	1.456	0.05	0.8	0.021	-5.8
	1.045	1.490	0.04	0.7	0.002	-4.9
O3…O4[1]	1.352	1.396	0.10	1.6	1.558	-14.4
	1.357	1.397	0.10	1.6	0.855	-14.1

[a] $\rho(\mathbf{r}_{CP})$ and $\nabla^2\rho(\mathbf{r}_{CP})$ are the electron density and the Laplacian values at the critical points (CP); ε is the ellipticity of the bond. E_{NC} (in kJ/mol) indicates the non-covalent interaction energy.
symmetry operations : [1]-x,-y, 2-z ; [2]1+x, y, z ; [3] x, y, z

Table 5. Integrated Atomic Charges (in e unit) in CBZ:ASP co-crystal. *EXP* and *TSF* correspond to the Refinements obtained from Experimental and Theoretical Structure Factors (TSF), respectively. "IAM" refers to the promolecule (Independent Atom Model) and "only" refers to molecules extracted from the crystal lattice.

	EXP CBZ in CBZ:ASP	*EXP CBZ only*	*IAM CBZ only*	*TSF CBZ in CBZ:ASP*	*TSF CBZ only*		*EXP ASP in CBZ:ASP*	*EXP ASP only*	*IAM ASP only*	*TSF ASP in CBZ:ASP*	*TSF ASP only*
C1	0.38	0.37	0.20	0.32	-0.07	**C16**	**1.11**	**0.75**	**0.76**	**1.00**	**0.75**
C2	-0.13	-0.10	-0.18	0.07	0.10	C17	0.22	0.11	-0.00	0.19	0.21
C3	-0.32	-0.33	-0.06	-0.17	-0.25	C18	-0.31	-0.02	-0.05	-0.25	-0.29
C4	0.11	0.10	-0.07	-0.07	-0.29	C19	-0.12	-0.20	-0.21	-0.38	0.04
C5	-0.19	-0.19	-0.10	-0.09	-0.05	C20	-0.27	-0.15	-0.15	-0.07	-0.13
C6	-0.04	-0.02	0.02	-0.15	0.17	C21	0.08	-0.04	-0.04	-0.21	-0.13
C7	-0.14	-0.08	-0.02	-0.04	-0.06	C22	0.15	0.31	0.05	0.40	0.37
C8	-0.13	-0.11	-0.06	-0.16	-0.42	**C23**	**1.50**	**0.97**	**0.74**	**1.09**	**1.16**
C9	0.23	0.22	0.11	0.04	0.20	**C24**	**-0.37**	**-0.36**	**-0.30**	**0.07**	**-0.45**
C10	0.08	0.09	-0.15	-0.14	-0.31	**O2**	**-0.71**	**-0.76**	**-0.76**	**-0.77**	**-0.79**
C11	-0.45	-0.43	-0.39	0.03	-0.06	**O3**	**-0.83**	**-0.46**	**-0.41**	**-0.85**	**-0.70**
C12	0.09	0.07	-0.33	-0.17	-0.43	**O4**	**-0.92**	**-0.63**	**-0.42**	**-0.46**	**-0.69**
C13	0.02	-0.02	0.01	0.02	-0.16	**O5**	**-1.11**	**-0.69**	**-0.59**	**-1.21**	**-0.87**
C14	0.04	0.00	0.17	0.17	0.24	H18	0.18	0.05	0.15	0.27	0.21
C15	**1.29**	**1.38**	**-0.10**	**1.62**	**0.86**	H19	0.15	0.08	0.16	0.24	0.05
N1	**-0.70**	**-0.64**	**-0.40**	**-0.98**	**-0.56**	H20	0.17	0.14	0.14	0.15	0.12
N2	**-0.98**	**-0.95**	**-0.83**	**-1.17**	**-1.00**	H21	0.06	-0.01	0.16	0.27	0.20
O1	**-0.71**	**-0.89**	**-0.69**	**-0.94**	**-0.93**	H22	0.08	0.16	0.15	0.08	0.29
H2	0.07	0.05	0.16	0.14	0.24	H23	0.14	0.03	0.15	0.04	0.17
H3	0.11	0.09	0.16	0.10	0.16	H24	0.13	0.11	0.17	0.16	0.16
H4	0.02	0.02	0.14	0.11	0.16	**H25**	**0.51**	**0.44**	**0.43**	**0.59**	**0.60**
H5	0.14	0.14	0.17	0.11	0.15						
H7	0.08	0.08	0.16	0.13	0.22						
H8	-0.02	-0.04	0.18	0.09	0.25						
H10	-0.10	-0.07	0.12	0.09	0.24						
H11	0.24	0.23	0.15	0.09	0.15						
H12	0.02	0.03	0.15	0.08	0.18						
H13	0.09	0.10	0.12	0.13	0.26						
H14	**0.45**	**0.43**	**0.33**	**0.50**	**0.53**						
H15	**0.40**	**0.37**	**0.33**	**0.47**	**0.47**						
Sum	-0.05	-0.10	-0.69	0.24	-0.02		-0.16	-0.17	0.13	0.33	0.28

Table 6. Electrostatic Potential at the Nuclei $V_{0,A}$ (EPN) from Experimental data (*EXP*) and from the Refinement of Theoretical Structure Factors (*TSF*). $V_{promol,A}$ is the EPN for the Independent Atom Model (*promolecule*). All values are in atomic unit.

	CBZ				*ASP*		
	$V_{promol,A}$	$V_{0,A,EXP}$	$V_{0,A,TSF}$		$V_{promol,A}$	$V_{0,A,EXP}$	$V_{0,A,TSF}$
C1	-14.690	-14.600	-14.761	C16	-14.690	-14.558	-14.722
C2	-14.690	-14.673	-14.696	C17	-14.690	-14.483	-14.719
C3	-14.690	-14.765	-14.821	C18	-14.690	-14.533	-14.733
C4	-14.690	-14.700	-14.863	C19	-14.690	-14.676	-14.652
C5	-14.690	-14.717	-14.808	C20	-14.690	-14.711	-14.728
C6	-14.690	-14.630	-14.713	C21	-14.690	-14.663	-14.738
C7	-14.690	-14.766	-14.758	C22	-14.690	-14.591	-14.688
C8	-14.690	-14.797	-14.799	**C23**	**-14.690**	**-14.545**	**-14.712**
C9	-14.690	-14.625	-14.649	**C24**	**-14.690**	**-14.636**	**-14.741**
C10	-14.690	-14.678	-14.786	**O2**	**-22.260**	**-22.139**	**-22.275**
C11	-14.690	-14.725	-14.778	**O3**	**-22.260**	**-22.126**	**-22.286**
C12	-14.690	-14.650	-14.850	**O4**	**-22.260**	**-22.165**	**-22.315**
C13	-14.690	-14.597	-14.787	**O5**	**-22.260**	**-22.013**	**-22.308**
C14	-14.690	-14.599	-14.678	H18	-1.000	-0.951	-0.938
C15	**-14.690**	**-14.524**	**-14.725**	H19	-1.000	-1.022	-1.036
N1	**-18.336**	**-18.193**	**-18.300**	H20	-1.000	-1.035	-1.057
N2	**-18.336**	**-18.318**	**-18.394**	H21	-1.000	-0.961	-0.961
O1	**-22.260**	**-22.203**	**-22.365**	H22	-1.000	-0.934	-0.931
H2	-1.000	-1.057	-1.007	H23	-1.000	-0.954	-0.991
H3	-1.000	-1.041	-1.073	H24	-1.000	-0.936	-1.022
H4	-1.000	-1.052	-1.045	**H25**	**-1.000**	**-0.865**	**-0.932**
H5	-1.000	-0.993	-1.058				
H7	-1.000	-1.078	-0.997				
H8	-1.000	-1.077	-1.010				
H10	-1.000	-1.074	-0.969				
H11	-1.000	-0.961	-1.019				
H12	-1.000	-1.043	-1.006				
H13	-1.000	-0.973	-0.959				
H14	**-1.000**	**-0.905**	**-0.964**				
H15	**-1.000**	**-0.934**	**-0.990**				

Table 7. Comparison of the Total Molecular Energies (in *hartree*) in CBZ:ASP Co-crystal Compared to Those in CBZ Form III. "Promolecule" refers to IAM and corresponds to energy derived from EPN. *CBZ···ASP, CBZ···CBZ are the dimers interacting through hydrogen bonds and CBZ/CBZ SH corresponds to the Sandwich Herringbone (SH) aromatic interactions.*

	CBZ:ASP co-crystal					
	RHF 6-31G**	***DFT B3LYP 6-31G*****	***DFT B3LYP cc-pvdz***	***EXP***	***TSF***	***Promolecule***
CBZ	-758.82	-763.12	-763.15	-762.18	-766.85	-763.44
ASP	-644.98	-648.36	-648.39	-644.14	-649.51	-648.57
CBZ···ASP	-1403.82	-1411.51	-1411.57	-1407.87	-1423.32	-1412.02
CBZ/CBZ SH	-1517.63	-1526.24	-1526.29	-1525.28	-1534.34	-1526.88
	CBZ III					
	RHF 6-31G**	***DFT B3LYP 6-31G*****	***DFT B3LYP cc-pvdz***	***EXP***	***TSF***	***Promolecule***
CBZ	-758.82	-763.12	-763.15	-771.92	-	-763.44
CBZ···CBZ	-1517.65	-1526.28	-1526.33	-1543.93	-	-1526.89
CBZ/CBZ SH	-1517.63	-1526.25	-1526.30	-1544.22	-	-1526.88

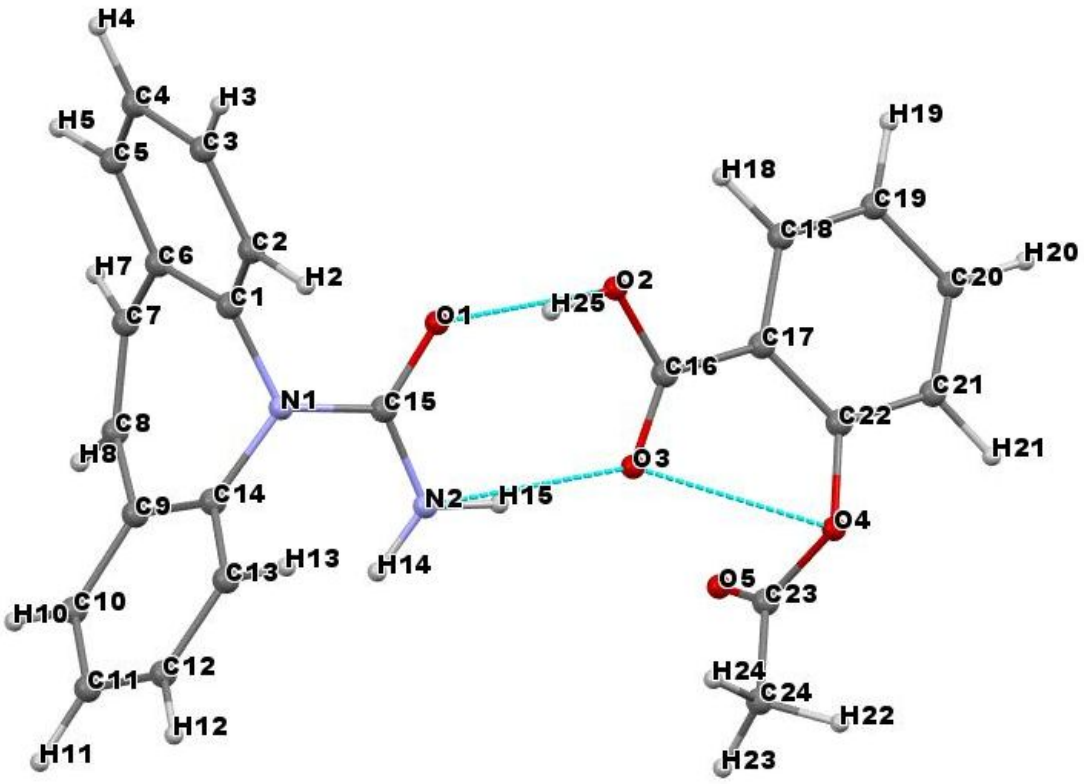

Figure 1. Molecular structure of CBZ:ASP with the numbering schemes of the atoms. Blue dotted lines indicate the hydrogen bonds.

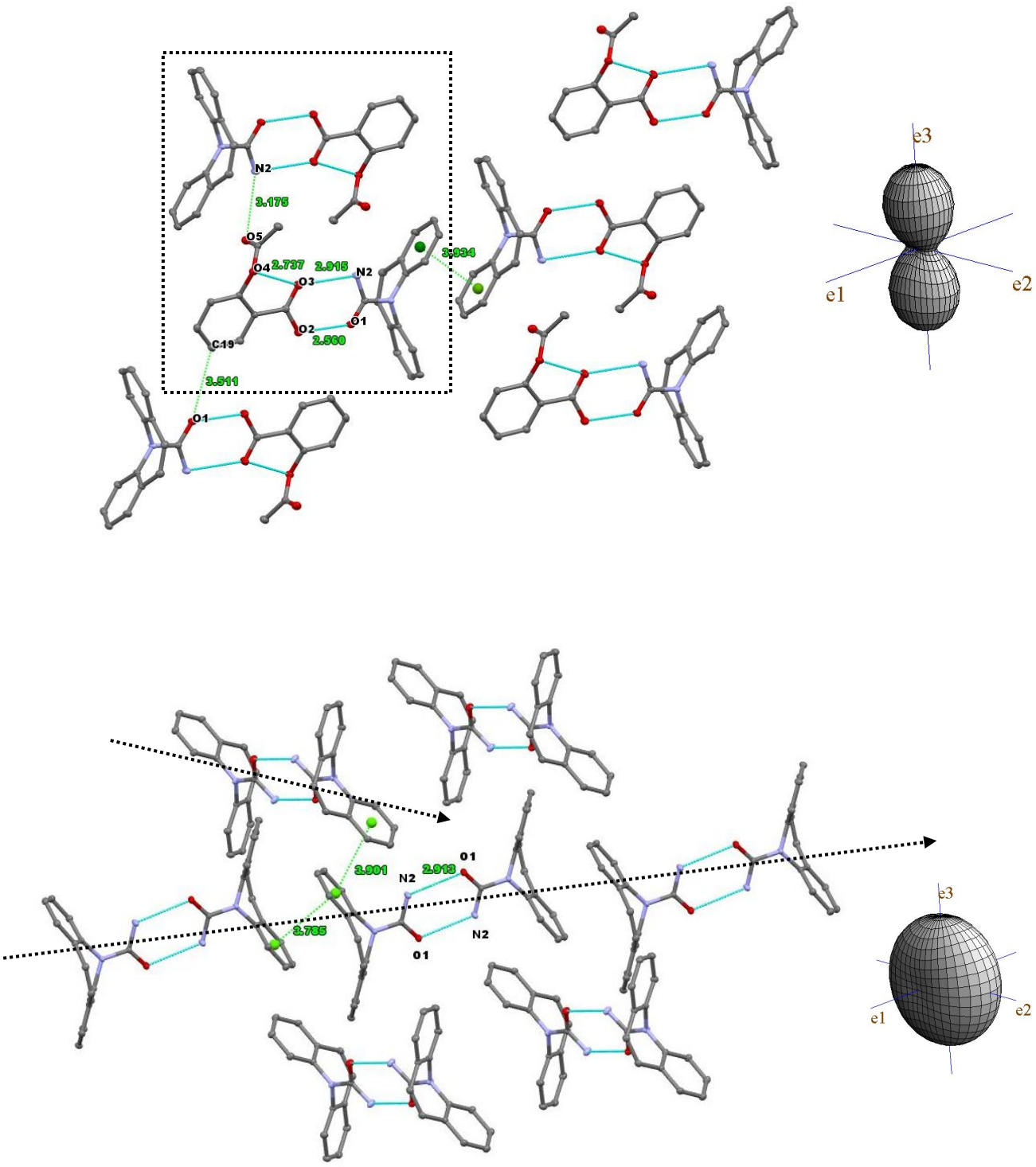

Figure 2. Molecular packing and hydrogen bonds in the crystal lattices of CBZ:ASP co-crystal (top) and CBZ III (bottom). H atoms are omitted. The main hydrogen bond (A-D) and benzene ring centroid-centroid distances are indicated in Å. The square in the CBZ:ASP structure groups together a quadrimer of interacting molecules, while in CBZ III structure, the lines indicate the two chains of aromatic group (SH) and H-bonds interactions. On the right column are given the graphical representation of the thermal expansion tensors of CBZ:ASP and CBZ III, $\mathbf{e}_1$, $\mathbf{e}_2$ and $\mathbf{e}_3$ are the principal directions of the tensors.

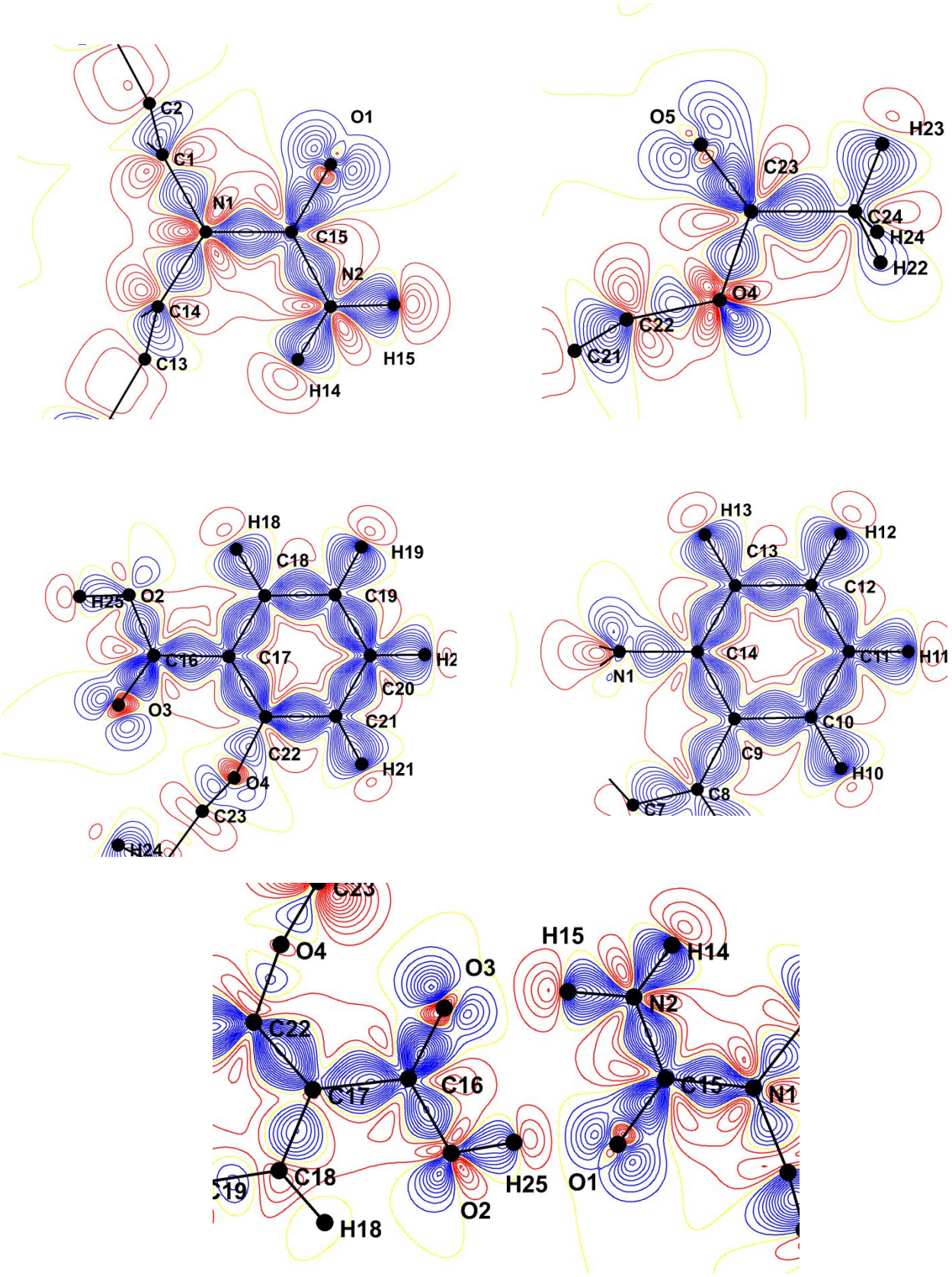

Figure 3. Experimental static electron deformation density in chosen planes of CBZ:ASP co-crystal. Contours are 0.05 eÅ^{-3}, positive contours are in blue and negative ones in red.

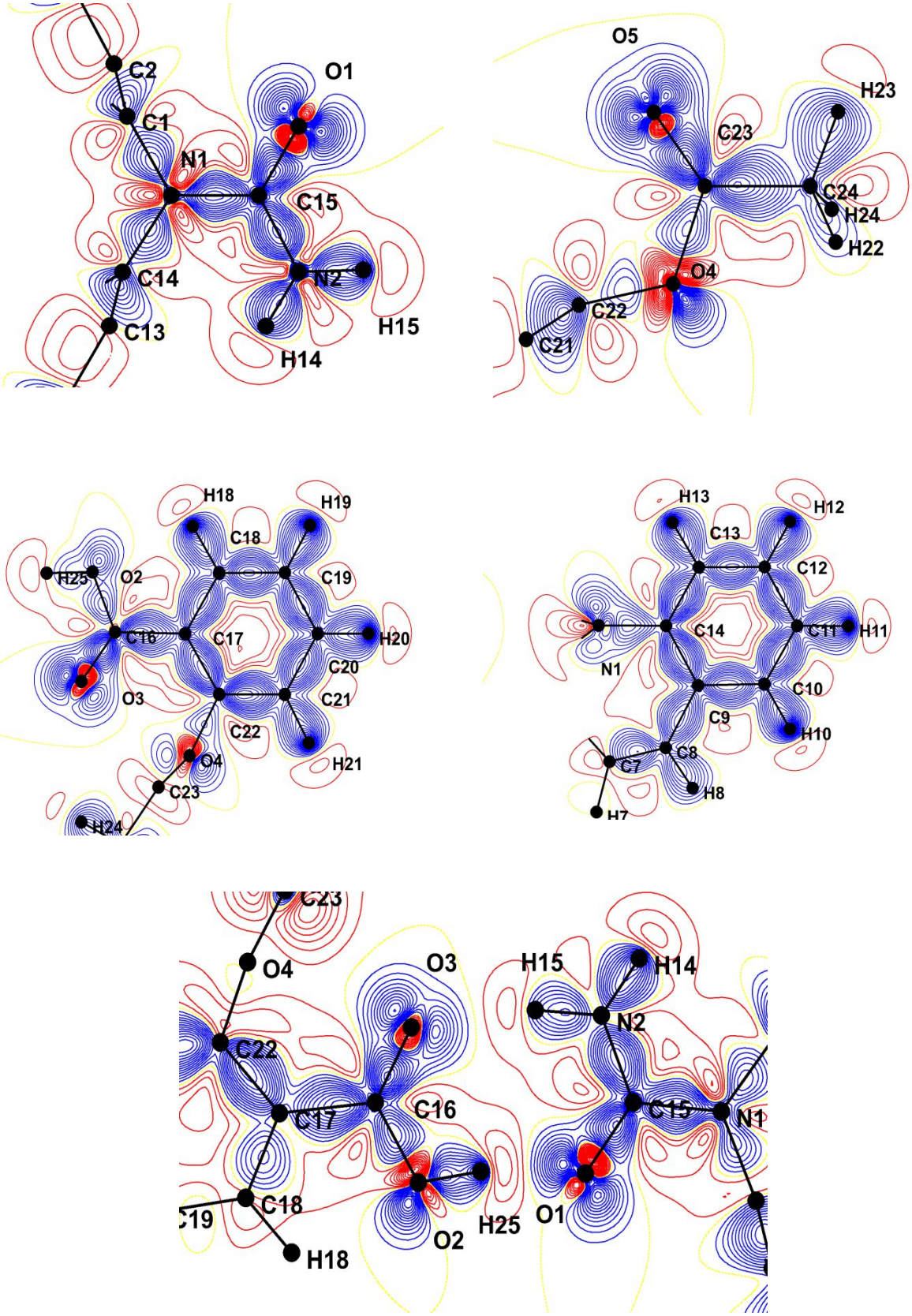
C2
O1
C1
N1
C15
C14
N2
C13
H15
H14
O5
H23
C23
C24
H24
H22
O4
C22
C21
H18
H19
C18
H25
O2
C19
C16
C17
H20
C20
O3
C21
C22
O4
H21
C23
H24
H13
H12
C13
C12
C14
C11
H11
N1
C10
C9
H10
C8
C7
H8
H7
C23
O4
O3
H15
H14
C22
N2
C17
C16
C15
N1
C19
C18
O2
H25
O1
H18

Figure 4. Static electron deformation density from the refinement of theoretical structure factors (TSF) in the same planes as in Figure 3 of CBZ-ASP co-crystal. Contours are 0.05 eÅ^{-3}, positive contours are in blue and negative ones in red.

CBZ

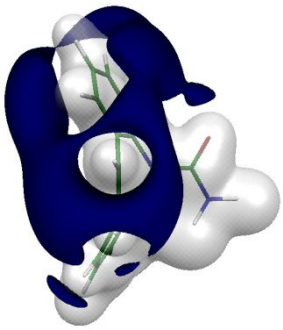

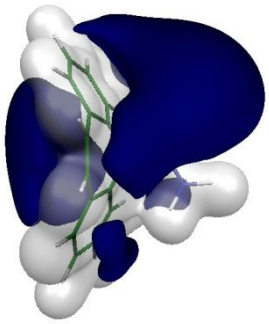

ASP

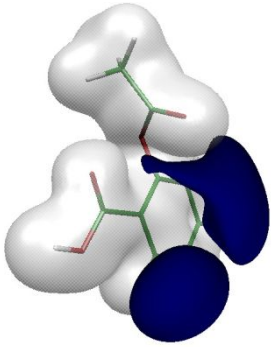

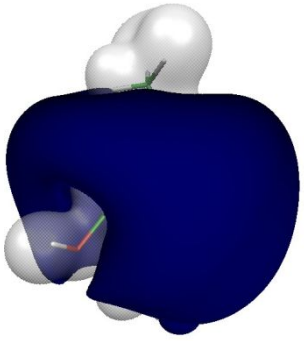

CBZ/CBZ (SH)

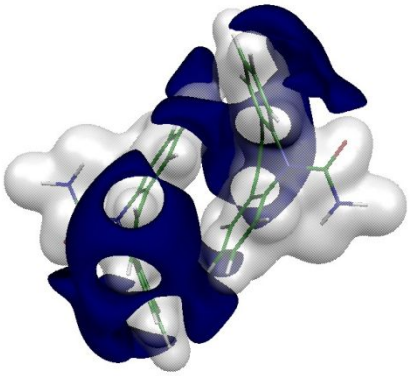

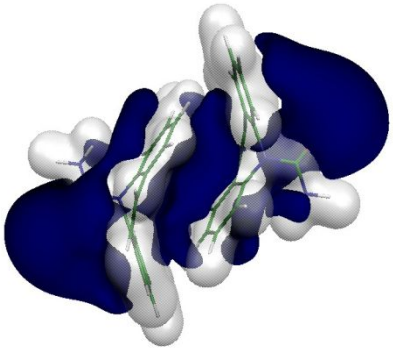

CBZ…ASP

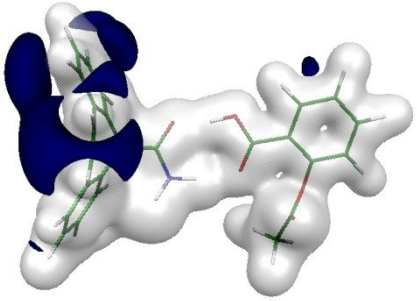

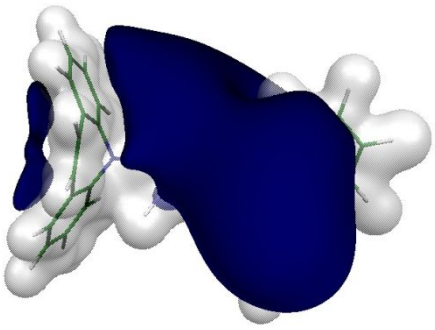

Figure 5. Electrostatic potential from experimental data (left column) and from the refinement of TSF (right column). Positive potential isosurface (+0.05 eÅ^{-1}) is in grey and the negative one (-0.03 eÅ^{-1}) is in blue.

For Table of Contents Use Only

Crystal and Electron Properties of Carbamazepine-Aspirin Co-crystal

Béatrice Nicolaï, Bertrand Fournier, Slimane Dahaoui, Jean-Michel Gillet and Nour-Eddine Ghermani

TOC

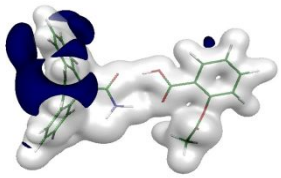

Synopsis

Experimental and theoretical charge densities of the carbamazepine-aspirin co-crystal have been derived from high-resolution X-ray diffraction and DFT cc-p*VDZ* basis set structure factors. Topological features of the electron density, atomic charges, electrostatic potential and total energy obtained from the electrostatic potential at the nuclei (EPN) are discussed.